STRUCTURAL SCIENCE
CRYSTAL ENGINEERING
MATERIALS

ISSN: 2052-5206
journals.iucr.org/b

Microwave-assisted synthesis and electrochemical evaluation of VO_2 (B) nanostructures

Thomas E. Ashton, David Hevia Borrás, Antonella Iadecola, Kamila M. Wiaderek, Peter J. Chupas, Karena W. Chapman and Serena A. Corr

Acta Cryst. (2015). B**71**, 722–726

STRUCTURAL SCIENCE
CRYSTAL ENGINEERING
MATERIALS

ISSN 2052-5206

Microwave-assisted synthesis and electrochemical evaluation of VO_2 (B) nanostructures

Thomas E. Ashton,[a] David Hevia Borrás,[a] Antonella Iadecola,[b,c,d] Kamila M. Wiaderek,[e] Peter J. Chupas,[e] Karena W. Chapman[e] and Serena A. Corr[a]*

[a]School of Chemistry, University of Glasgow, Glasgow G12 8QQ, Scotland, [b]The European Synchrotron, 71 Avenue des Martyrs, 38000 Grenoble, France, [c]Reseau sur le Stockage Electrochimique de l'Energie, FR CNRS 3459, France, [d]Synchrotron SOLEIL, L'Orme des Merisiers, 91192, Saint Aubin, Gif sur Yvette France, and [e]X-ray Science Division, Argonne National Laboratory, 9700 South Cass Avenue, Argonne, Illinois 60439, USA. *Correspondence e-mail: serena.corr@glasgow.ac.uk

Received 7 September 2015
Accepted 9 November 2015

Edited by R. I. Walton, University of Warwick, England

Keywords: vanadium dioxide; Li-ion battery; X-ray absorption spectroscopy; *in-situ*; intercalation.

Understanding how intercalation materials change during electrochemical operation is paramount to optimizing their behaviour and function and *in situ* characterization methods allow us to observe these changes without sample destruction. Here we first report the improved intercalation properties of bronze phase vanadium dioxide VO_2 (B) prepared by a microwave-assisted route which exhibits a larger electrochemical capacity (232 mAh g^{-1}) compared with VO_2 (B) prepared by a solvothermal route (197 mAh g^{-1}). These electrochemical differences have also been followed using *in situ* X-ray absorption spectroscopy allowing us to follow oxidation state changes as they occur during battery operation.

1. Introduction

As global energy demands continue to increase, much attention has been dedicated to the improvement of electrochemical storage devices such as Li-ion batteries (Bruce *et al.*, 2008; Goodenough & Kim, 2010; Masquelier & Croguennec, 2013). One way in which performance can be enhanced is to improve the electrochemical capacity of the active electrode (Rangappa *et al.*, 2012; Li & Zhou, 2012). This might be achieved by reducing the electrode particle dimensionality, where smaller sizes lead to a decrease in Li^+ diffusion pathlengths thus aiding the intercalation process. Judicious choice of synthesis route can lead to materials of a desired shape and size. In the case of the bronze phase VO_2 (B), the synthesis route employed can lead to changes in particle shape, size and morphology affording nanobelts, nanowires, hollow microspheres or mesoporous structures with varied electrochemical performance (Qin *et al.*, 2014; Corr *et al.*, 2009; Armstrong *et al.*, 2008; Kong *et al.*, 2012; Niu *et al.*, 2014; Zhang *et al.*, 2014; Mai *et al.*, 2013). For example, capacities of around 150 mAh g^{-1} are observed in bulk materials (Zhang & Dahn, 1996) and nanosheets (Li *et al.*, 2015), 265 mAh g^{-1} in ultrathin nanowires (Armstrong *et al.*, 2008) and 325 mAh g^{-1} in nanocrystals (Tsang & Manthiram, 1997). The vanadium oxides (V_xO_y) represent an interesting class of intercalation electrodes due to their highly tuneable oxidation state chemistry, with many V_xO_y compounds already investigated as electrode materials including V_2O_5 (Cao *et al.*, 2005), V_6O_{13} (Lampe-Önnerud *et al.*, 1995; Zou *et al.*, 2014), LiV_3O_8 (Liu *et al.*, 2009) and the bronze phase VO_2(B) (Pan *et al.*, 2013). VO_2 (B) is a promising candidate electrode material due to its competitive theoretical capacity of 323 mAh g^{-1} for one Li^+ ion per formula unit, compared with $LiCoO_2$ (272 mAh g^{-1})

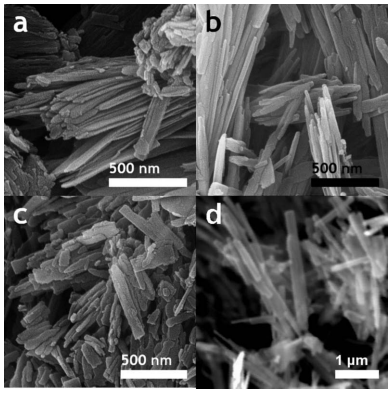

and $LiFePO_4$ (170 mAh g^{-1}) (Mizushima *et al.*, 1980). The solvothermal method is commonly employed to obtain nanostructured VO_2 (B), taking up to several days to complete (Corr *et al.*, 2009). Therefore, a fast, reliable method to achieve these nanostructured materials with good electrochemical performance would be desirable. Recently, microwave-assisted solvothermal routes have been applied for the rapid synthesis of intercalation materials such as $LiCoO_2$ and $LiFePO_4$ (Subramanian *et al.*, 2001; Zeng *et al.*, 2013; Ashton *et al.*, 2014). The effectiveness of the microwave-assisted solvothermal approach is governed by the selection of reactants or solvents that can efficiently absorb and convert the microwave irradiation into heat. While there have been limited reports of the use of microwave-assisted routes for the preparation of vanadate materials (Li *et al.*, 2013; Beninati *et al.*, 2006; Arbizzani *et al.*, 2007; Prado-Gonjal *et al.*, 2013), there has been no systematic study of their preparation and subsequent electrochemical properties.

X-ray absorption spectroscopy (XAS) is a powerful tool for uncovering oxidation states, coordination environments and local structural information of a particular atomic species of interest. The use of such a technique on intercalation electrodes allows direct analysis of the structural and electronic behaviour transition metals during electrochemical charge/discharge (Yoon *et al.*, 2003). Investigating this behaviour is an important step in fully understanding the intercalation chemistry of electrode materials. We report for the first time the microwave-assisted synthesis of nanostructured VO_2 (B), the differences in electrochemical capacity of VO_2(B) synthesized by both solvothermal and microwave-assisted routes, and the evolution of the V^{4+}/V^{3+} redox couple by *in situ* XAS during battery operation.

2. Experimental

2.1. Synthesis of VO_2 (B)

Samples of VO_2 (B) were prepared by the solvothermal [ST48h] and microwave-assisted [MW1h, MW3h and MW6h] reduction of V_2O_5 in formaldehyde solution. ST48h was prepared by adding V_2O_5 (1.81 g, 10 mmol) to formaldehyde solution (30 ml, 37% in H_2O) in a 45 ml Teflon lined steel autoclave and heating to 453 K for 48 h. The microwave samples were prepared by adding V_2O_5 (0.3 g, 1.65 mmol) to formaldehyde solution (15 ml, 37%) in a 35 ml glass reaction vessel which was irradiated with microwaves in a CEM Discover SP microwave synthesizer (2.45 GHz) at 454 K, 1 h (MW1h), 3 h (MW3h) and 6 h (MW6h). The resulting black powders were washed with water, ethanol and acetone and dried in an oven overnight at 343 K. Structural characterization was carried out by powder X-ray diffraction (XRD) using a PANalytical X'pert Pro diffractometer with Cu $K\alpha_1$ source in Bragg–Brentano configuration, and scanning electron microscopy (SEM) using a Carl Zeiss Sigma variable pressure analytical electron microscope equipped with a Schottky thermal field emitter at 20 kV and an in-lens secondary electron detector.

2.2. Electrochemical measurements

Cathode pellets containing 60% active material (ST48h or MW3h), 30% carbon black and 10% PTFE binder were prepared by grinding together in an agate mortar and pressing at 1.2 tonne. The pellets were placed onto a stainless steel current collector inside battery cells constructed using stainless steel Swagelok® housing electrically insulated with Mylar. The cathode was then covered with a glass wool separator and soaked with electrolyte ($LiPF_6$ in a 1:1 v:v ratio of ethylene carbonate and dimethyl carbonate). A disc of Li metal was placed on the separator as the anode and the battery stack was compressed with a spring loaded stainless steel current collector. All work was carried out in an Ar-filled glovebox.

2.3. *In situ* X-ray absorption spectroscopy

In situ X-ray absorption spectra were collected using an AMPIX battery cell (Borkiewicz *et al.*, 2012). Pellets of the cathode material containing 30% active material (ST48h or MW3h), 25% VULCAN® nanocarbon (Cabot), 25% graphite powder and 20% PTFE binder were pressed at 1.2 tonne and placed on the glassy carbon window/current collector. The pellet was covered by a disc of Celgard® film and Kapton® foam disc as a separator and soaked with electrolyte before adding the lithium metal anode. All work was carried out in an Ar-filled glovebox. Vanadium K-edge absorption measurements were performed at the BM23 beamline of the ESRF synchrotron radiation facility, Grenoble, where the synchrotron radiation emitted by a

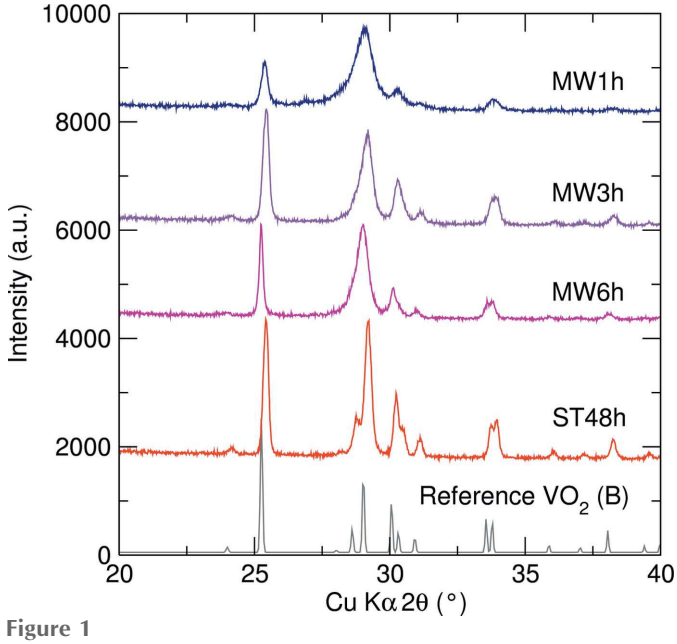

Figure 1
Powder XRD patterns of products from solvothermal synthesis ST48h (red) and microwave-assisted synthesis MW6h (pink), MW3h (purple) and MW1h (blue) show an increase in peak broadening with decreasing reaction time. A reference pattern for VO_2 (B) is also included from Oka *et al.* (1993) [space group; $C12/m1$, a = 12.093 (1), b = 3.7021 (2), c = 6.4330 (5) Å, α = 90, β = 106.97 (1), γ = 90°].

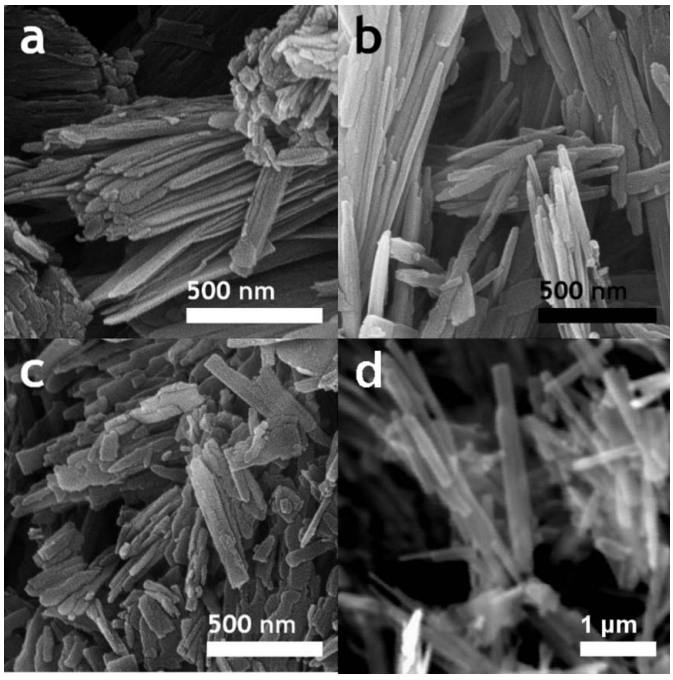

Figure 2
SEM images of (*a*) [MW1h], (*b*) 3 h [MW3h] and (*c*) 6 h [MW6h] and (*d*) [ST48h].

bending magnet source was monochromated using a double crystal Si(111) monochromator. The data were collected in the transmission mode using three ionization chambers mounted in a series for simultaneous measurements on the sample and a vanadium foil as reference. ST48h and MW3h were studied *in situ*, while discharging the batteries at a C/20 rate (insertion of 1 Li^+ per formula unit in 20 h) after an initial full discharge up to 3.8 V using a Biologic VSP potentiostat. XAS data was extracted and normalized using the *Athena* software package (Ravel & Newville, 2005) using edge-step normalization.

3. Results and discussion

Materials prepared from the solvothermal reaction (ST48h, 48 h reaction) and microwave-assisted reactions (MW1h, MW3h and MW6h for 1, 3 and 6 h treatments respectively) were characterized using powder XRD (Fig. 1). Sample ST48h can be indexed to a single phase bronze VO_2 (space group $C12/m1$), as previously reported by Corr *et al.* (2009). For the samples prepared using microwave irradiation as the heat source, an increase in peak broadening is observed in all cases and Fig. 1 shows this broadening increases with decreasing reaction time. This may indicate increasing crystallite size with increasing microwave treatment time, which is further shown from the measured FWHM for each pattern (values of 0.68, 0.48 and 0.46° for MW1h, MW3h and MW6h samples, respectively).

SEM images of the VO_2 (B) samples confirm a change in particle size with reaction heat treatment and time (Fig. 2). For ST48h, similar sizes are observed as those previously reported (typically, ~ 1.2 µm long, 150 nm wide). In the case of samples prepared using the microwave-assisted approach, the particle length decreases from ~ 1 µm to 800 nm on going from 6 h to 1 h treatment times. The typical particle width also increases for increased reaction times, going from 100 nm for MW1h to 150 nm for MW6h.

In order to investigate whether this morphological difference has an impact on the resulting electrochemical performance, galvanostatic cycling experiments were performed using ST48h and MW3h as active positive electrodes cycled against Li metal between 3.8 and 1.8 V (Fig. 3*a*). It is observed that we can reversibly intercalate more Li^+ per formula unit into MW3h compared with ST48h. A corresponding increase in discharge capacity is noted, 197 mAh g^{-1} for ST48h and 232 mAh g^{-1} for MW3h. This agrees well with observations in the literature that decreasing particle sizes lead to increased capacities, with our values for ST48h and MW3h lying between those for bulk (150 mAh g^{-1}) and ultra-thin nanowires (265 mAh g^{-1}) of VO_2 (B). The stability at higher current densities was also investigated (Fig. 3*b*). It is observed that the MW3h sample delivers consistently higher capacities than the ST48h sample retaining 85 and 90% of their initial capacities, respectively. The largest loss in capacity is observed at rates above 2C.

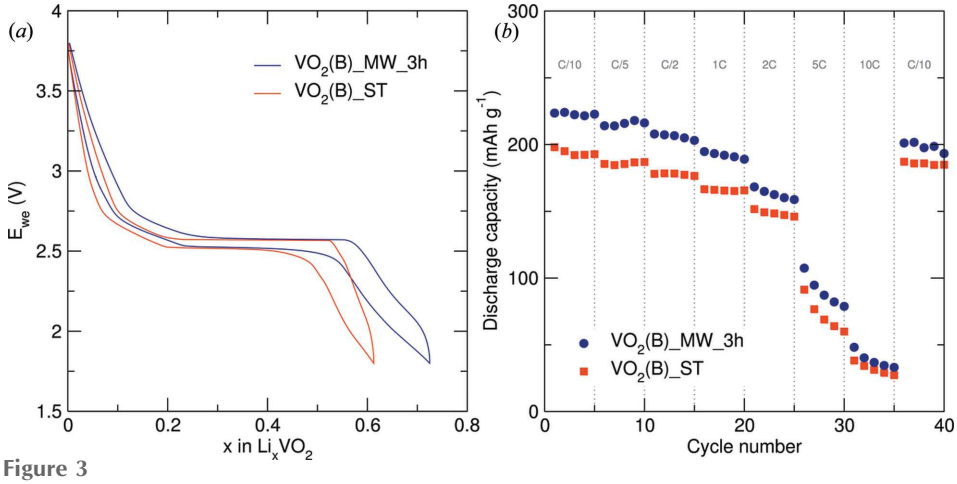

Figure 3
(*a*) Galvanostatic cycling with potential limitation profile from the first discharge–charge cycle of ST48h and MW3h from 1.8 V to 3.8 V at a C/20 rate. (*b*) Discharge capacities of the galvanostatic cycling with potential limitation for the ST48h and MW3h samples at rates from C/10 to 10C.

To further understand the differences in intercalation behaviour in these materials, *in situ* X-ray absorption spectra (XAS) at the vanadium K-edge were recorded during electrochemical discharge. Firstly XAS spectra were collected for several vanadium standards [V^{3+} (V_2O_3), V^{4+} (VC) and V^{5+} (V_2O_5)], and of ST48h,

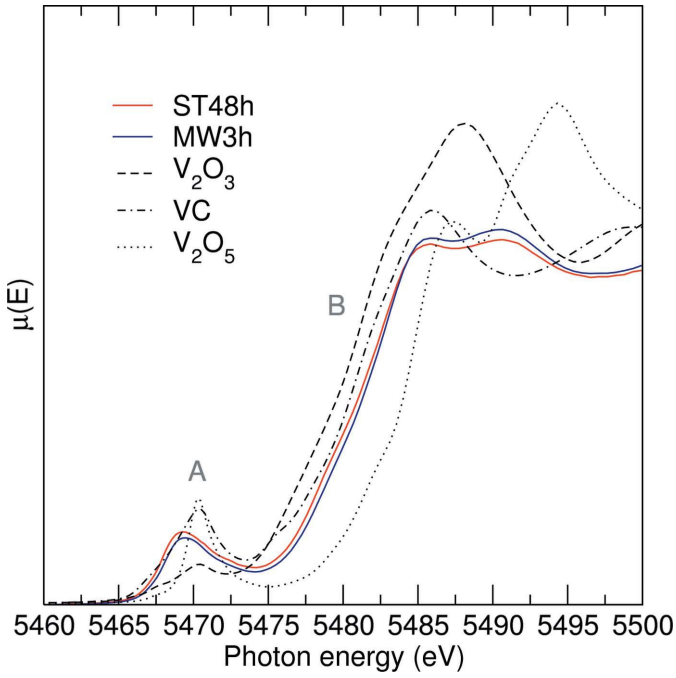

Figure 4
Normalized XAS spectra of the V K-edge for microwave-assisted (MW3h) and solvothermally prepared (MW48h) VO_2 (B) samples with standards of vanadium in different oxidation states from 3+ to 5+. Features A and B denote the pre-edge and rising edge, respectively.

MW3h *ex situ* (Fig. 4). The X-ray absorption near-edge structure (XANES) presents two characteristic features A and B, respectively, at lower energy and the rising edge. It is known that feature A is mainly characterized by a strong contribution due to the 1*s*–3*d* quadrupole transition (Wu *et al.*, 2004), here at 5467 eV. On the other hand, peak B is due to the 1*s*–empty 4*p* dipole transition. With decreasing oxidation state, the spectra of the standards shift to lower energy due to the loss of one electron and the destabilization of the 1*s* orbital with respect to the outer vanadium *d* and *p* orbitals. The pre-edge peak *A* is an indicator of a lack of centrosymmetry as the 1*s* to 3*d* transition would usually be forbidden. However, distortion of VO_6 polyhedra in these materials leads to *d*/*p* orbital mixing and hence a transition can occur and is observed for ST48h and MW3h. The rising edge of the VO_2 (B) samples lies between that of the V^{3+} and V^{5+} standards close to the V^{4+} standard indicating an expected initial oxidation state of V^{4+}.

In situ XAS measurements were recorded of samples ST48h and MW3h discharging at a constant current of 20 μA between 3.8 and 1.8 V. The vanadium K-edge of the active material was scanned continuously. Spectra reveal a shift in the rising edge of the spectra from 5482.0 eV to lower energies with increasing Li^+ concentration for both ST48h and MW3h (Figs. 5*a* and *c*, respectively). As Li^+ is inserted into the VO_2 (B) structure, the pre-edge feature decreases in intensity. The first derivative plots for both materials show a new shoulder is formed in the pre-edge upon lithiation which is due to the emergence of V^{3+}, from the reduction of V^{4+}, confirming the presence of both oxidation states concurrently. Previous studies by Wong *et al.* (1984) have shown that the pre-edge energy of the vanadates increases linearly with increasing oxidation state at a rate of 1.1 eV. If we assume this linearity is preserved *between* oxidation states, we observe a maximum of 0.4 Li per formula unit is intercalated in our studies and thus expect a shift of approximately −0.44 eV. For Li_xVO_2, where $x = 0.40$, we observe a shift to lower energy in the order of −0.35 eV for ST48h and −0.55 for MW3h. This implies that, given the similar experimental conditions, we have a greater reduction of V^{4+} in MW3h compared with ST48h over the same cycling regime. From this, we can conclude that the smaller particle size makes it easier for Li^+ intercalation in the case of the microwave sample which accounts for the higher discharge capacity in MW3h. This behaviour is also consistent with the shift observed in the rising edge, where ST48h exhibits a shift of approximately 1 eV and MW3h approximately 1.3 eV. The profile at the peak of the rising edge is also dramatically different in ST48h (double peaked) and MW3h (single peaked), which may be a result of different structural changes occurring, mediated by particle morphology.

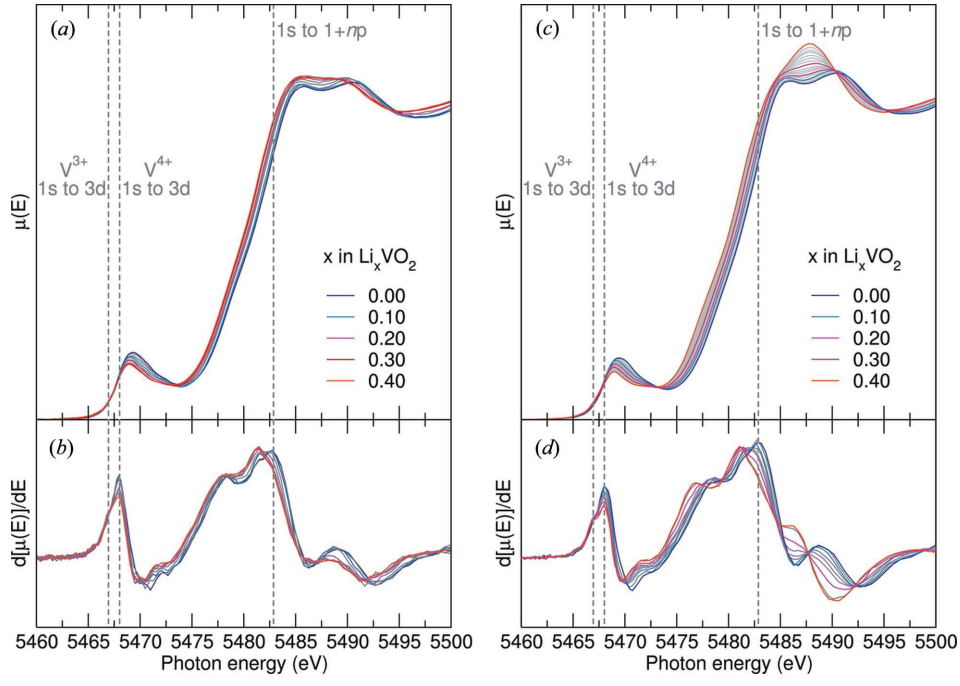

Figure 5
In situ X-ray absorption spectroscopy collected at the V K-edge during electrochemical discharge of (*a*) ST48h and (*c*) MW3h and their derivatives (*b*) and (*d*), respectively.

4. Conclusions

Our microwave synthetic approach reliably and reproducibly yields gram-scale quantities of nanostructured VO_2 (B) with improved electrochemical performance over VO_2 (B) synthesized by a conventional solvothermal route. The reason for this electrochemical difference has been explained by a link to the morphology, where smaller particle dimensions lead to increased capacity. Our *in situ* XAS measurements have proven that there is a link between electrochemical capacity and the behaviour of the V^{4+}/V^{3+} redox couple as particle sizes are reduced. Further investigations are required to link structural changes to those observed in oxidation state of the material, however, XANES analysis has given an interesting insight into the behaviour of vanadium oxides as intercalation electrodes.

Acknowledgements

We gratefully acknowledge helpful discussions with Dr Mark Newton and technical support from Mr Michael Beglan. We also thank the European Radiation Synchrotron Facility (ESRF) for beam time allocation, the EPSRC (EP/K029290/1 and EP/N001982/1) and Royal Society (RG100301) for funding, the University of Glasgow for support and the School of Chemistry for the use of its facilities. Work done at Argonne and use of the Advanced Photon Source, an Office of Science User Facility operated for the US Department of Energy Office of Science by Argonne National Laboratory, were supported by the US Department of Energy under Contract No. DE-AC02-06CH11357.

References

Arbizzani, C., Beninati, S., Damen, L. & Mastragostino, M. (2007). *Solid State Ionics*, **178**, 393–398.
Armstrong, G., Canales, J., Armstrong, A. R. & Bruce, P. G. (2008). *J. Power Sources*, **178**, 723–728.
Ashton, T. E., Laveda, J. V., MacLaren, D. A., Baker, P. J., Porch, A., Jones, M. O. & Corr, S. A. (2014). *J. Mater. Chem. A*, **2**, 6238–6245.
Beninati, S., Fantuzzi, M., Mastragostino, M. & Soavi, F. (2006). *J. Power Sources*, **157**, 483–487.
Borkiewicz, O. J., Shyam, B., Wiaderek, K. M., Kurtz, C., Chupas, P. J. & Chapman, K. W. (2012). *J. Appl. Cryst.* **45**, 1261–1269.
Bruce, P. G., Scrosati, B. & Tarascon, J.-M. (2008). *Angew. Chem. Int. Ed.* **47**, 2930–2946.
Cao, A. M., Hu, J. S., Liang, H. P. & Wan, L. J. (2005). *Angew. Chem. Int. Ed.* **44**, 4391–4395.
Corr, S. A., Grossman, M., Shi, Y. F., Heier, K. R., Stucky, G. D. & Seshadri, R. (2009). *J. Mater. Chem.* **19**, 4362–4367.
Goodenough, J. B. & Kim, Y. (2010). *Chem. Mater.* **22**, 587–603.
Kong, F. Y., Li, M., Yao, X. Y., Xu, J. M., Wang, A. D., Liu, Z. P. & Li, G. H. (2012). *CrystEngComm*, **14**, 3858–3861.
Lampe-Önnerud, C., Nordblad, P. & Thomas, J. O. (1995). *Solid State Ionics*, **81**, 189–199.
Li, J. M., Chang, K. H., Wu, T. H. & Hu, C. C. (2013). *J. Power Sources*, **224**, 59–65.
Li, L., Liu, P., Zhu, K., Wang, J., Liu, J. & Qiu, J. (2015). *J. Mater. Chem. A*, **3**, 9385–9389.
Li, H. & Zhou, H. (2012). *Chem. Commun.* **48**, 1201–1217.
Liu, H. M., Wang, Y. G., Wang, K. X., Wang, Y. R. & Zhou, H. S. (2009). *J. Power Sources*, **192**, 668–673.
Mai, L. Q., Wei, Q. L., An, Q. Y., Tian, X. C., Zhao, Y. L., Xu, X., Xu, L., Chang, L. & Zhang, Q. J. (2013). *Adv. Mater.* **25**, 2969–2973.
Masquelier, C. & Croguennec, L. (2013). *Chem. Rev.* **113**, 6552–6591.
Mizushima, K., Jones, P. C., Wiseman, P. J. & Goodenough, J. B. (1980). *Mater. Res. Bull.* **15**, 783–789.
Niu, C. J., Meng, J. S., Han, C. H., Zhao, K. N., Yan, M. Y. & Mai, L. Q. (2014). *Nano Lett.* **14**, 2873–2878.
Oka, Y., Yao, T., Yamamoto, N., Ueda, Y. & Hayashi, A. (1993). *J. Solid State Chem.* **105**, 271–278.
Pan, A. Q., Wu, H. B., Yu, L. & Lou, X. W. (2013). *Angew. Chem. Int. Ed.* **52**, 2226–2230.
Prado-Gonjal, J., Molero-Sánchez, B., Ávila-Brande, D., Morán, E., Pérez-Flores, J. C., Kuhn, A. & García-Alvarado, F. (2013). *J. Power Sources*, **232**, 173–180.
Qin, M. L., Liang, Q., Pan, A. Q., Liang, S. Q., Zhang, Q., Tang, Y. & Tan, X. P. (2014). *J. Power Sources*, **268**, 700–705.
Rangappa, D., Murukanahally, K. D., Tomai, T., Unemoto, A. & Honma, I. (2012). *Nano Lett.* **12**, 1146–1151.
Ravel, B. & Newville, M. (2005). *J. Synchrotron Rad.* **12**, 537–541.
Subramanian, V., Chen, C. L., Chou, H. S. & Fey, G. T. K. (2001). *J. Mater. Chem.* **11**, 3348–3353.
Tsang, C. & Manthiram, A. (1997). *J. Electrochem. Soc.* **144**, 520–524.
Wong, J., Lytle, F. W., Messmer, R. P. & Maylotte, D. H. (1984). *Phys. Rev. B*, **30**, 5596–5610.
Wu, Z. Y., Xian, D. C., Hu, T. D., Xie, Y. N., Tao, Y., Natoli, C. R., Paris, E. & Marcelli, A. (2004). *Phys. Rev. B*, **70**, 033104.
Yoon, W. S., Grey, C. P., Balasubramanian, M., Yang, X. Q. & McBreen, J. (2003). *Chem. Mater.* **15**, 3161–3169.
Zeng, G., Caputo, R., Carriazo, D., Luo, L. & Niederberger, M. (2013). *Chem. Mater.* **25**, 3399–3407.
Zhang, M. J. & Dahn, J. R. (1996). *J. Electrochem. Soc.* **143**, 2730–2735.
Zhang, L., Zhao, K. N., Xu, W. W., Meng, J. S., He, L., An, Q. Y., Xu, X., Luo, Y. Z., Zhao, T. W. & Mai, L. Q. (2014). *RSC Adv.* **4**, 33332–33337.
Zou, Z. G., Cheng, H., He, J. Y., Long, F., Wu, Y., Yan, Z. Y. & Chen, H. X. (2014). *Electrochim. Acta*, **135**, 175–180.